Contents lists available at ScienceDirect

Arabian Journal of Chemistry

journal homepage: www.ksu.edu.sa

Original article

# Doped-MXene assists in deciphering metabolic signature of psoriasis and unraveling dysregulated leukotriene metabolism

Jun Chen [a,b], Fang Liu [b], Haibo Liu [b], Tengrui Wang [c], Yun Hui [b], Huan Chen [b], Qingtao Kong [b,*]

[a] The Fourth Affiliated Hospital of Nanjing Medical University, Department of Dermatology, Nanjing 211500, China
[b] Jinling Hospital, Affiliated Hospital of Medical School, Nanjing University, Nanjing, 210002, China
[c] School of Materials and Engineering, Tongji University, Shanghai 200090, China

ARTICLE INFO

*Keywords:*
Doped MXene
Metabolic signature
Psoriasis
Dysregulated leukotriene metabolism

ABSTRACT

Psoriasis, characterized by erythematous plaques, desquamation, persistent pruritus, and discomfort, significantly compromises the quality of life for afflicted individuals. The intricate interplay of immunological, genetic, and environmental factors has left the molecular intricacies of psoriasis only partially elucidated, underscoring the imperative to unravel these intricate mechanisms. In contradistinction to conventional techniques such as nuclear magnetic resonance (NMR) and liquid chromatography-mass spectrometry (LC-MS), the burgeoning laser desorption/ionization (LDI) metabolic paradigm holds substantial promise in elucidating the molecular mechanism of psoriasis. Nonetheless, achieving heightened sensitivity and high-throughput metabolite detection within intricate clinical biosamples mandates stringent requisites, encompassing favourable ionization efficiency and high surface area. Henceforth, we proffered a dual-strategy entailing the utilization of transition metal carbides (MXene) with unique morphology and the integration of multi-walled carbon nanotubes (MWCNTs) to ameliorate these challenges for psoriasis. We have corroborated the morphological architecture, elemental composition, and efficacy of LDI when applied to MWCNTs-doped MXene. Egregiously, through the employment of both animal models and clinical specimens, we attained diagnostic efficiencies of 0.959 and 0.924 via receiver operating characteristic (ROC) curve analysis, respectively, for discrimination psoriasis from control individuals. Doped MXene evinced exceptional signal amplification and imperviousness to salt and protein interference. Furthermore, enrichment pathway analysis unveiled a significant escalation in leukotriene E4 and arachidonic acid levels within the psoriasis cohort. Harnessing LDI metabolic fingerprints, concomitant with MWCNTs-doped MXene, expedited the recognition of the distinct metabolic characteristics inherent to psoriasis, thereby laying bare the dysregulation in leukotriene metabolism. This epochal breakthrough holds immense potential to usher in new vistas for exploring the underlying mechanisms governing the onset and progression of psoriasis-related disorders, thereby significantly contributing to the refinement of psoriasis health management strategies.

## 1. Introduction

Psoriasis, a chronic dermatologic ailment, profoundly compromises patients' life quality, instigating cutaneous manifestations like desquamation, pruritus, and erythematous lesions, and even precipitating systemic complications such as arthritic conditions (Raharja et al., 2021; Zhou et al., 2022). The precise etiology of psoriasis remains enigmatic, entwined within intricate factors encompassing immunological, genetic, and environmental dimensions, thereby necessitating a further expeditious course of research and exploration (Hu et al., 2021; Raharja et al., 2021; Sotiriou et al., 2021). In juxtaposition to the domains of proteomics and genomics, metabolomics serves as a direct conduit to delineate the metabolic milieu intrinsic to the biological matrix, thereby furnishing an all-encompassing and veracious portrayal of the aberrant metabolic signatures underpinning psoriasis, thereby affording a profound illumination of the substructure governing the ailment's pathogenic tapestry (Gao et al., 2018; Wang et al., 2023; Wu and Zhao, 2019). Consequently, the prospect of pioneering novel metabolomic methodologies augurs to proffer a revelatory glimpse into the inception and progression of psoriasis, thereby unfurling unexplored vistas for

Peer review under responsibility of King Saud University.
* Corresponding author.
*E-mail address:* njukqt@163.com (Q. Kong).

https://doi.org/10.1016/j.arabjc.2024.105774
Received 6 October 2023; Accepted 2 April 2024
Available online 3 April 2024

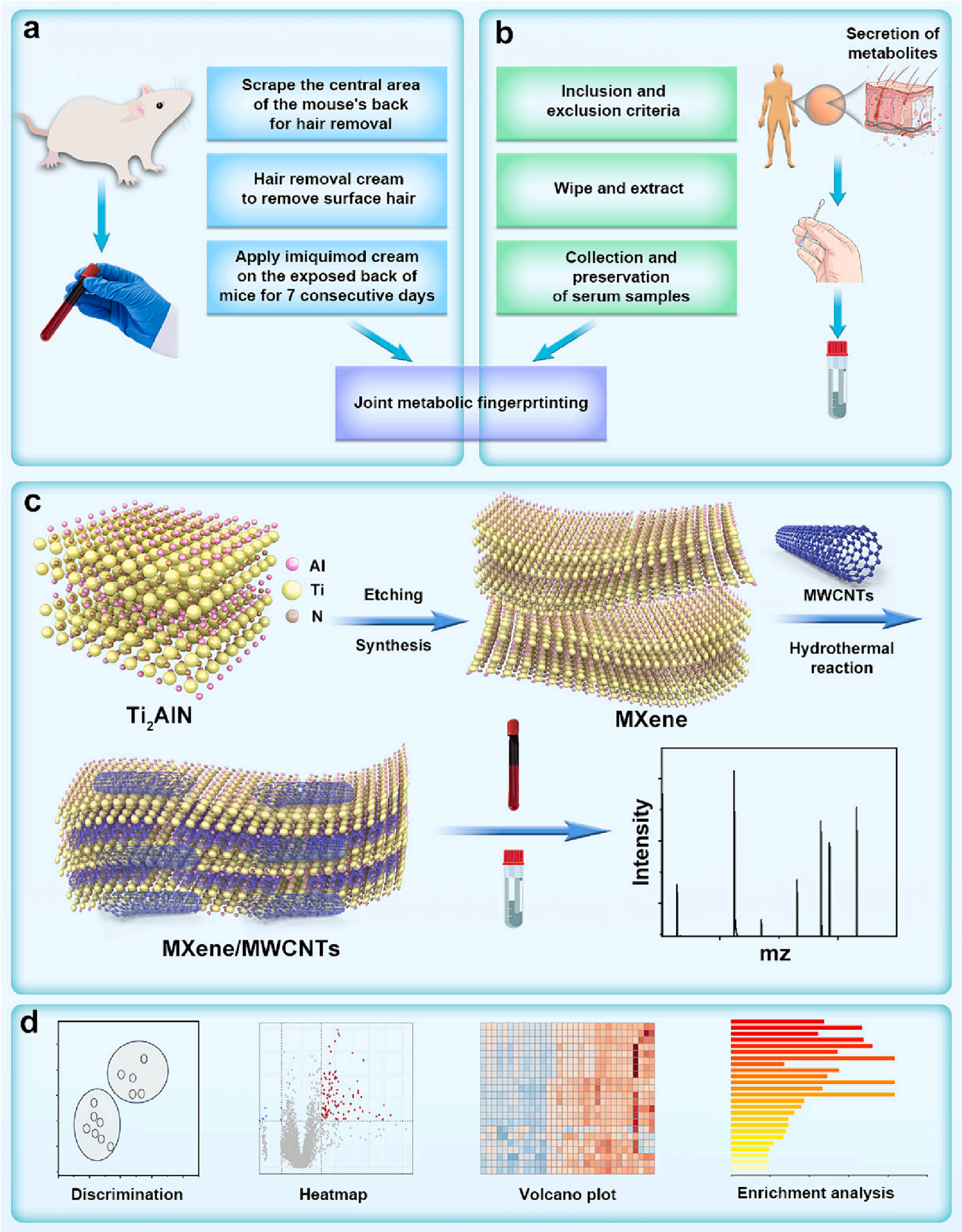


**Fig. 1.** Comprehensive metabolomic strategy leveraging MXene/MWCNTs matrix for psoriasis investigation. a) Sequential phases encompassing metabolomic analysis on animal model samples. b) Meticulous profiling of metabolomic analysis on clinical psoriasis skin samples. c) Intricate synthesis and proficient utilization of MXene ene/MWCNTs nanomaterial. d) Strategic employment of diverse metabolomic analysis techniques, encompassing OPLS-DA, heatmaps, volcano plots, and enrichment analysis.

advancing its biomolecular mechanism oversight.

Matrix-assisted laser desorption/ionization (MALDI) technology, characterized by heightened sensitivity, expeditious analytical kinetics, and compatibility with high-throughput metabolomic interrogations, is a vanguard in large-scale metabolomic investigations (Hamdi et al., 2017; Kailasa and Wu, 2015; Wang et al., 2020). Unlike nuclear magnetic resonance (NMR) spectroscopy and liquid chromatography-mass spectrometry (LC-MS), the MALDI technique dispenses with intricate pre-analytical procedures, expeditiously conferring insight into the metabolic tableau. The veritable fruition of MALDI pivots on judicious matrix selection, with the matrix material orchestrating the absorption of laser energy and concomitantly catalyzing the ionization cascade of analyte molecules, thus intricately influencing the fidelity and sensitivity of the analytical verdict. MXene, an emergent two-dimensional assemblage of metal, carbon, and nitrogen, augments this discourse with its exceptional conductive attributes and biocompatibility, thereby endowing it with propitious prospects in biomedicine (Jiang et al., 2021; Li et al., 2020; Naguib et al., 2012). In the ambit of laser desorption/ionization (LDI) techniques, MXene unfurls an array of advantages, including its two-dimensional architecture and pronounced conductive propensity, synergistically potentiating laser photon absorption, thereby expediting the ionization and desorption kinetics of analyte species, thereby culminating in an augmentation of the sensitivity quotient intrinsic to LDI (Chen et al., 2021; Hosseini et al., 2020; Li et al., 2020; Yang et al., 2020). Besides, The laminar structure and high lattice stability of MXene confer favorable stability and durability within the biological environment. Moreover, MXene's commingling of biocompatibility and surface energetics augments its potential for applications in the realm of biometric analysis, thereby positioning it as an auspicious vector for the role of matrix material. Simultaneously, the hybridization of MXene presents an augmentation of laser energy absorption, magnifying the efficacy of laser-induced ionization, albeit with the caveat of lingering challenges on judicious hybridization strategies and material design nuances. The multi-walled carbon nanotubes (MWCNTs), epitomizing high electrical conductivity and expansive surface area, emerge as prime candidates for ameliorating LDI efficacy, accentuating the quantum of incident light absorption and the efficiency of ion generation for analyte species (Mugo and Alberkant, 2020; Wang et al., 2018), ultimately culminating in an elevation of the LDI sensitivity and overall efficiency. Furthermore, the singular architecture and chemical attributes inherent to MWCNTs substantiate their role as a resilient conduit for energy transduction and spectral performance, thus endowing them with the pedigree to serve as a substantive matrix material. Consequently, the blueprint for the hybrid integration of two-dimensional MXene constructs with MWCNTs emerges as a tantalizing frontier, heralding the advent of an efficacious paradigm for the systematic unravelling of psoriasis aetiology.

In this work, we have developed a metabolomics methodology employing MWCNTs-doped two-dimensional MXene-assisted laser ablation mass spectrometry to delve profoundly into the molecular mechanisms of psoriasis, as depicted in Fig. 1. To begin, we established a psoriasis animal model by treating mouse skin with imiquimod, as outlined in Fig. 1a. Subsequently, we extracted metabolites from skin samples for subsequent metabolomics analysis. Concurrently, employing stringent criteria differentiating psoriasis patients from healthy controls, we selected 32 skin samples from healthy individuals and 38 from psoriasis patients. These samples were then subjected to skin scraping and extraction of metabolic products for blood metabolomics analysis, as represented in Fig. 1b. Moreover, we fabricated two-dimensional MXene materials through sodium hydroxide etching and amalgamated them with MWCNTs via hydrothermal synthesis, yielding a matrix material tailored for metabolomics applications, as showcased in Fig. 1c. Ultimately, an array of analytical strategies encompassing Orthogonal partial least squares discriminant analysis (OPLS-DA), heatmap, volcano plot, and enrichment analysis will be harnessed to unravel the intricate molecular mechanisms of psoriasis, as illustrated in Fig. 1d. This comprehensive approach holds the promise of furnishing theoretical insights into the fundamental guidance underlying the occurrence and development mechanisms of psoriasis.

Therefore, we have orchestrated a metabolomic schema underscored by MWCNTs-infused MXene matrices for LDI, designed to expound the molecular edifice of psoriasis aetiology. We have adroitly substantiated the two-dimensional configuration and elemental composition of MWCNTs-imbued MXene, thereby corroborating the augmentation of its LDI performance. We have garnered diagnostic efficiencies of 0.959 and 0.924 for psoriasis and control groups by harnessing the synergy of animal models and clinical specimens. Augmented by enrichment pathway analysis, the conspicuous overexpression of leukotriene E4 and arachidonic acid in the psoriasis cohort underscored their significance. The congruent validation of enzyme-mRNA expression related to these metabolic cascades corroborates a constructive correlation, propounding a conjecture that the dysregulation of leukotriene metabolism might orchestrate the psoriatic pathology, thereby furnishing a peephole into comprehending the ontogeny of psoriasis and potentially enriching the canvas of therapeutic interventions.

## 2. Materials and methods

### 2.1. Synthesis of MXene/MWCNTs

Using Ti powder, Al powder, and C powder as raw materials, with a molar ratio of Ti:Al:C = 3:1.2:2.1, the raw materials are mixed uniformly after ball milling for 10–20 h (Eom et al., 2020; J. Zhang et al., 2019; Zhu et al., 2020). The mixture is then sealed in a boron nitride or graphite crucible and placed in a SiC tube furnace with flowing Ar gas as a protective atmosphere. The temperature is ramped up at a rate of 10 ~ 40 °C/min to reach 1300 ~ 1450 °C. Subsequently, the mixture undergoes a solid–liquid phase reaction for 0.5 ~ 4 h at the corresponding temperature. This method of invention offers high product purity, short reaction time, uniform particle size distribution, convenient operation, and a simple process. The synthesized 3.0 g $Ti_3ALC_2$, 0.01 g sodium fluoride (NaF) and 0.1 g multi-walled carbon nanotubes (purchased from Chengdu Organic Chemistry Co., Ltd., Chinese Academy of Sciences) are dissolved in 10 mL of 1 M sodium hydroxide solution (Shang et al., 2020; Zeng et al., 2020; Zhang et al., 2020). The mixture is subjected to hydrothermal etching under ultrasonic conditions for 8 h. Afterwards, the solution is centrifuged three times, and the corresponding product is collected. The final synthesized MXene/MWCNTs are stored in a refrigerator at 4 °C.

### 2.2. Animal model of psoriasis

The mouse model induced by imiquimod (IMQ), is widely applied for research purposes (Pinget et al., 2022; Zhang et al., 2021). It not only effectively replicates the cutaneous manifestations of psoriasis-like lesions but also exhibits intrinsic immune dysregulation and acquired immune responses similar to psoriasis. This model is preferred due to its ease of manipulation, high success rate, and extensive utilization in literature. The specific modelling procedure is as follows: Carefully remove the fur from the central area of the mouse's back, creating an exposed area measuring 2 cm × 3 cm. Apply a mild depilatory cream to remove the surface fuzz. Apply 5 % imiquimod (62.5 mg per application for the 2 cm × 3 cm skin area) continuously to the mouse's back skin for 5 to 10 days. Evaluate the skin condition daily and collect serum samples from successfully modelled mice for subsequent psoriasis metabolomics analysis.

### 2.3. H&E staining

To begin, place the mouse in an appropriate anaesthetic environment and induce anaesthesia using isoflurane. Once the mouse is completely anaesthetized, secure its back using tape or clamps. Proceed to cleanse

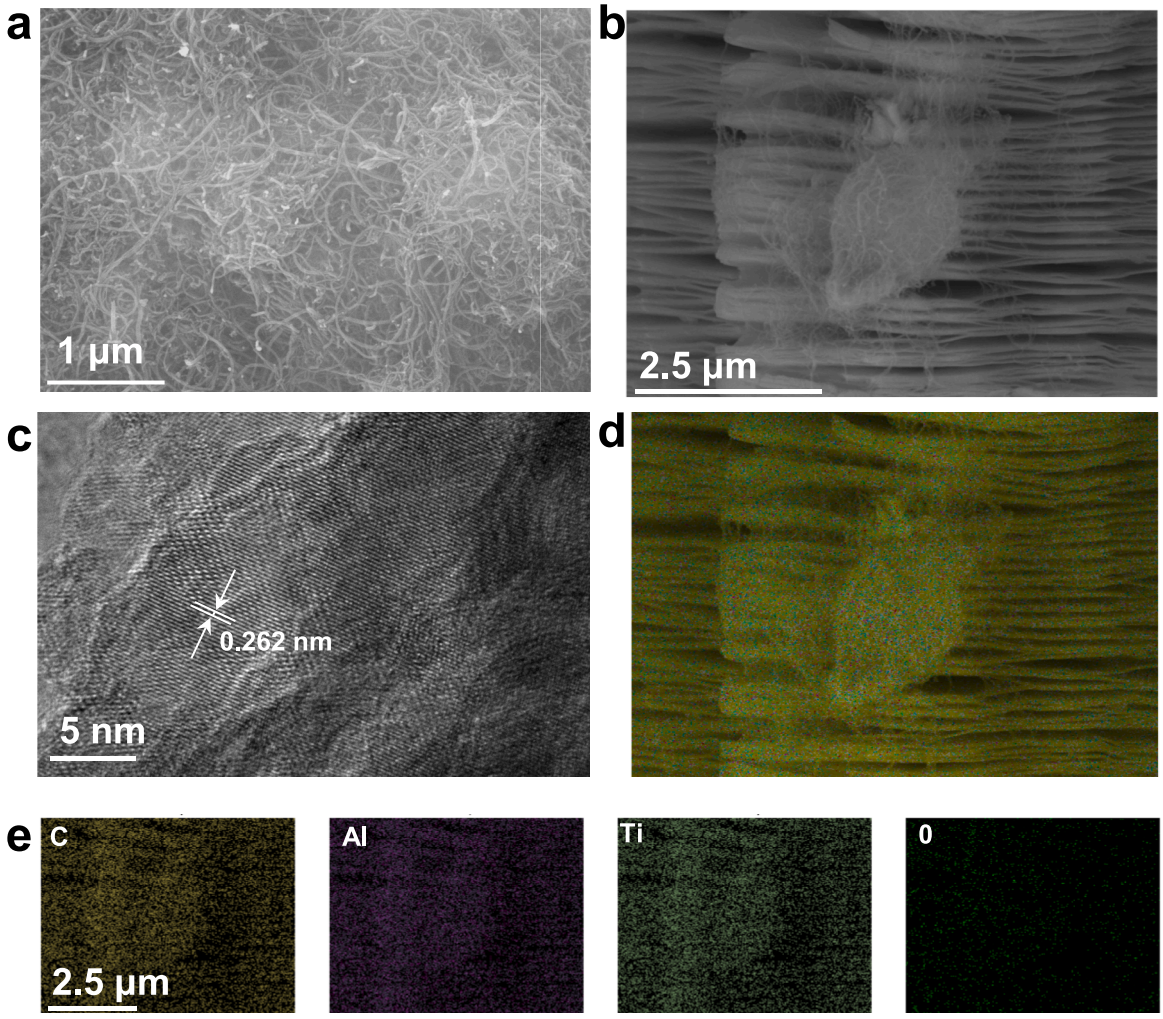


**Fig. 2.** Morphology and elemental characterizations of MXene/MWCNTs. a) SEM image of MWCNTs. b) SEM analysis of MXene/MWCNTs displayed a distinctive morphology where multi-walled carbon nanotubes were encapsulated within its layered structure. c) TEM analysis of MXene/MWCNTs. d-e) Mapping analysis of MXene/MWCNTs, including elements C, Al, Ti, and O.

the skin surface with a disinfectant, ensuring a sterile environment. Gently remove the hair from the central region of the mouse's back using medical scissors and forceps, revealing the underlying epidermal tissue. If needed, cautiously utilize a surgical scalpel to retrieve thin slices of the epidermal tissue. Following this, process the fixed skin sample into sections via deparaffinization and dehydration. Immerse the sections in a hematoxylin solution, resulting in cell nuclei staining in varying shades of purple and blue. Subsequently, engage in destaining and bluing steps to heighten the clarity of nuclear staining. Proceed by staining the sections with the acidophilic eosin dye, imparting pink hues to the cytoplasm and extracellular structures. Lastly, prepare the tissue sections for microscopic examination by undergoing dehydration, clearing, and slide mounting procedures (Lai et al., 2018; Y. Zhang et al., 2019).

### 2.4. Metabonomics analysis

Metabolomics analysis encompasses techniques such as Principal Component Analysis (PCA), Orthogonal Partial Least Squares Discriminant Analysis (OPLS-DA), heatmaps, volcano plots, and enriched pathway identification, facilitated through MetaboAnalyst 5.0 (https://www.metaboanalyst.ca/). The processing of high-throughput mass spectrometry data necessitates preprocessing, peak alignment, and calibration procedures.

### 2.5. Validation of 5-LO and LCT4s

In the pursuit of mRNA testing for 5-LO and LTC4s, an initial step involved the extraction of total RNA from the samples. This was succeeded by the process of reverse transcription, facilitated by the utilization of a reverse transcriptase enzyme to effectuate the synthesis of cDNA. Following this, primers that held a complementary affinity for the target mRNA sequences were meticulously designed, thereby underpinning the subsequent stages. The preparatory phase included the establishment of specialized PCR reaction systems. Employing a thermal cycler as the vehicle, the amplification phase ensued, characterized by a tripartite temperature progression encompassing denaturation, annealing, and extension. After the amplification process, the resultant PCR products were subjected to meticulous analysis via agarose gel electrophoresis. This analytical method facilitated a discerning comparison with discerning molecular weight markers, the purpose of which was to definitively corroborate the presence of the desired PCR products specific to the designated targets.

### 2.6. LDI detection and characterizations and XRD analysis

The LDI testing for MXene, MWCNTs, and MXene/MWCNTs involved the utilization of 100 μg/mL concentrations of creatinine and phenylalanine. For assessing protein tolerance, a mixture of standard solutions

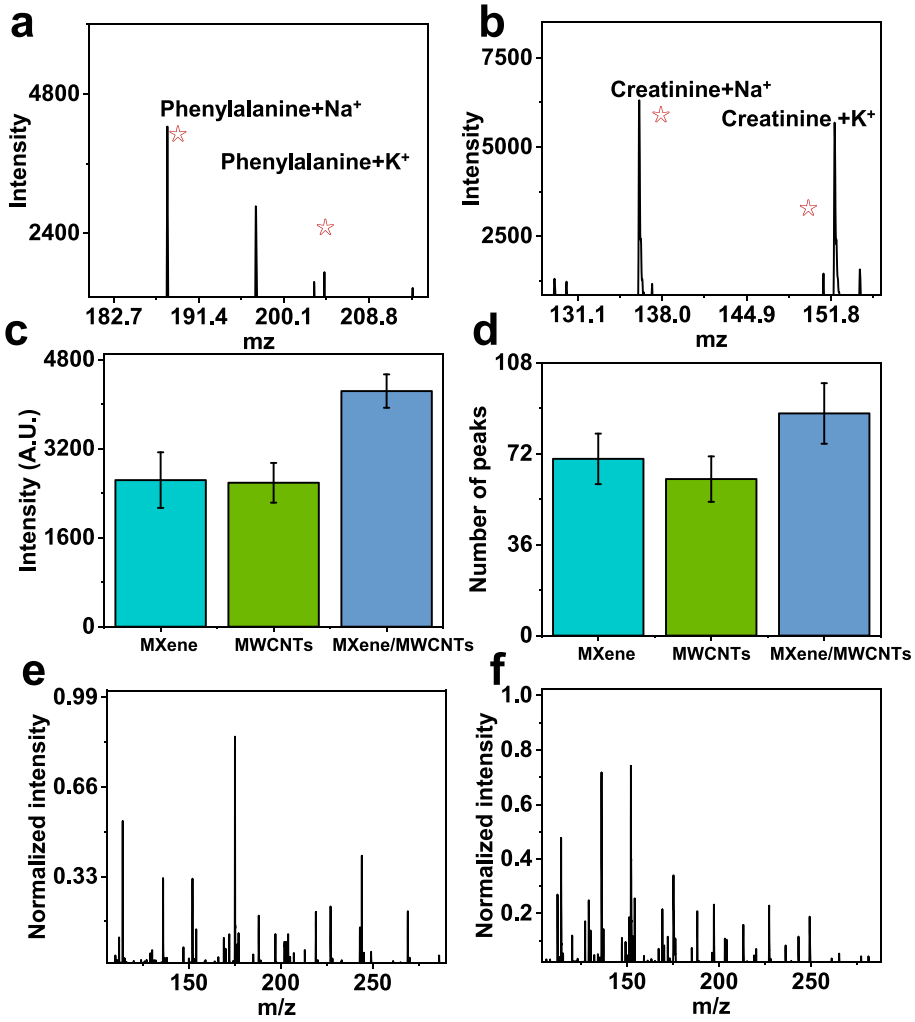


**Fig. 3.** Performance evaluation of MXene/MWCNTs for LDI-MS. Performance of MXene/MWCNTs as LDI matrix for detecting a) phenylalanine and b) creatinine. c) Detection intensity statistics for MXene, MWCNTs, and MXene/MWCNTs, and d) Peak number statistics for MXene, MWCNTs, and MXene/MWCNTs in clinical samples. The detection performance of MXene, MWCNTs, and MXene/MWCNTs for standard samples includes e) protein tolerance and f) salt tolerance.

and 10 mg/mL bovine serum albumin was employed. To evaluate salt tolerance, standard solutions were blended with 5.0 mg/mL NaCl. The XRD analysis was conducted using a Rigaku Miniflex instrument with CuKα radiation (λ = 1.54060 Å) and a scanning rate of 2θ/m. The 2θ range spanned from 5° to 60° during the analysis.

## 3. Results and discussion

### 3.1. Morphology and elemental characterization of MXene/MWCNTs

The judicious selection of an appropriate matrix material assumes paramount significance within metabolite detection, particularly in the intricate context of biological samples like serum. In the pursuit of achieving high-throughput capabilities and exceptional sensitivity, the efficacy of matrix materials in ionization and laser transmission assumes a pivotal role in governing the expansive scope of metabolite detection. Therefore, we have chosen MXene materials with a layered structure as the foundational material for LDI metabolite detection. MXene (Fig.S1a-e, Fig.S2, Table S1) exhibited a unique two-dimensional morphology, and its layered structure facilitates the laser desorption ionization of various metabolites on its surface. We also conducted X-ray diffraction (XRD, Fig.S1f) analysis on the synthesized MXene material and found that the peaks at 18.57° and 29.2° correspond to the (006) and (008) characteristic peaks, consistent with the literature (Malik et al., 2022), which effectively validated the successful synthesis of the MXene. To further optimize its performance, we selected multi-walled carbon nanotubes (MWCNTs, Fig. 2a) with excellent laser transmission efficiency for modification through a hydrothermal reaction. MXene/MWCNTs displayed a distinctive morphology where multi-walled carbon nanotubes were encapsulated within its layered structure (Fig. 2b). TEM analysis of MXene/MWCNTs (Fig. 2c) revealed a lattice spacing of 0.026 nm, which is consistent with prior literature (Abbasi et al., 2021). Furthermore, we conducted a mapping analysis of MXene/MWCNTs (Fig. 2d, Fig S3), and elemental analysis including C, Al, Ti, and O confirmed the elemental composition (Fig. 2e, Fig. S4). In summary, our SEM and TEM characterizations effectively validated the morphology and elements of MXene/MWCNTs, laying the foundation for future applications.

### 3.2. Performance evaluation of MXene/MWCNTs for LDI-MS

The meticulous assessment of the matrix material's performance in metabolomic analysis plays a pivotal role, particularly when delving into the intricacies of psoriasis. Consequently, a thorough evaluation was undertaken to comprehend the matrix's efficacy. As illustrated in Fig. 3a-b, the successful identification of phenylalanine and creatinine using MXene/MWCNTs, accompanied by the emergence of discernible sodium and potassium peaks, unequivocally affirmed the potential of

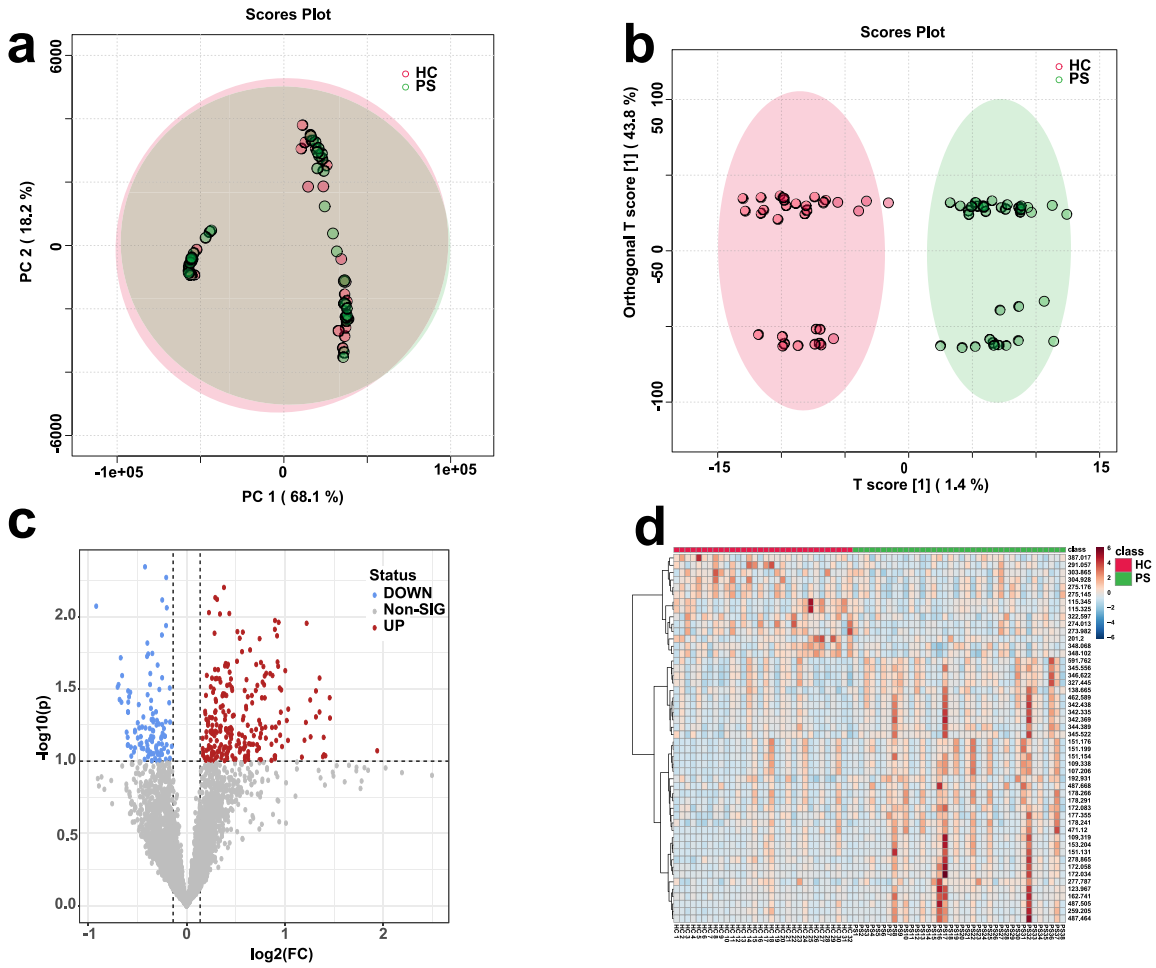


**Fig. 4.** LDI-MS-based metabolomic fingerprinting of clinical psoriasis skin samples using MXene/MWCNTs. a) PCA and b) OPLS-DA analyses distinguishing control and psoriasis groups. c) Volcano plot analysis of 32 control and 38 psoriasis skin biosamples, with blue and red representing downregulated and upregulated molecules, respectively. d) Heatmap analysis of control and psoriasis groups, highlighting the differences between the two groups.

MXene/MWCNTs in detecting standard samples. With meticulous refinement, integrating MWCNTs into MXene demonstrated elevated sensitivity. Specifically, the peak intensity of MXene/MWCNTs (2635 ± 318, Fig. 3c) increased by 60.6 % compared to pure MXene (3547 ± 498) and 64.3 % compared to pristine MWCNTs (2587 ± 357). Moving onward, the capacity of MXene/MWCNTs to discern an increased number of peaks within clinical sample detection was unveiled, an invaluable attribute when confronted with the intricacy of analyzing multifaceted clinical samples. Especially, the number of peaks for MXene/MWCNTs increased from 70 ± 10, as depicted in MXene, and 62 ± 9, as seen in MWCNTs, to 88 ± 11 (Fig. 3d). Furthermore, MXene/MWCNTs exhibited exceptional tolerance to proteins (Fig. 3e) and salts (Fig. 3f), fortifying its utility. The comprehensive validation of standard samples, optimization, protein tolerance, and salt tolerance collectively underscored the practicality of MXene/MWCNTs as an LDI matrix material, subsequently laying the groundwork for upcoming psoriasis metabolomic analyses.

### 3.3. *LDI-MS-based metabolomic fingerprinting of psoriasis using MXene/MWCNTs*

In the pursuit of comprehending the intricate tapestry of psoriasis, it becomes imperative to discern it from the backdrop of control groups. This elucidation provides a gateway to uncover the unique metabolic perturbations intrinsic to psoriasis. Accordingly, we embarked on a multifaceted exploration, encompassing skin and animal model serum biosamples, thereby approaching psoriasis from diverse angles. In Fig. 4a, we delineated our concerted efforts to gather skin samples from healthy individuals and psoriasis patients (Table S3). Blood extraction through meticulous scraping sets the stage for the subsequent metabolomic analysis. Employing a judicious combination of principal component analysis (PCA) and orthogonal partial least squares discriminant (OPLS-DA), as showcased in Fig. 4a-b, we efficaciously discerned between the skin samples sourced from 32 healthy individuals and those from 38 individuals grappling with psoriasis. These distinctions paved the way for the embodiment of molecular alterations in the form of upregulated and downregulated shifts, expertly presented through volcano plots in Fig. 4c. These plots serve as intuitive visualizations, encapsulating the essence of metabolite variations under distinct conditions. Akin to a symphony of data, heatmaps in Fig. 4d unfold a mesmerizing visual panorama that accentuates the intricate metabolic disparities between skin samples originating from healthy individuals and psoriasis patients. These heatmaps, adeptly deciphering complex multidimensional information, offer a window of insight into potential biomarkers and biological interconnections, augmenting our comprehension of the meaningful significance of metabolites. Through these endeavours, the synergy of methodologies such as OPLS-DA, volcano plots, and heatmaps contributes profoundly to the intricate analysis and discovery of biomarkers within psoriasis skin samples, thereby unravelling pivotal insights into the molecular underpinnings governing the evolution and progression of this enigmatic malady.

Transitioning our exploration, we delve into the realm of serum

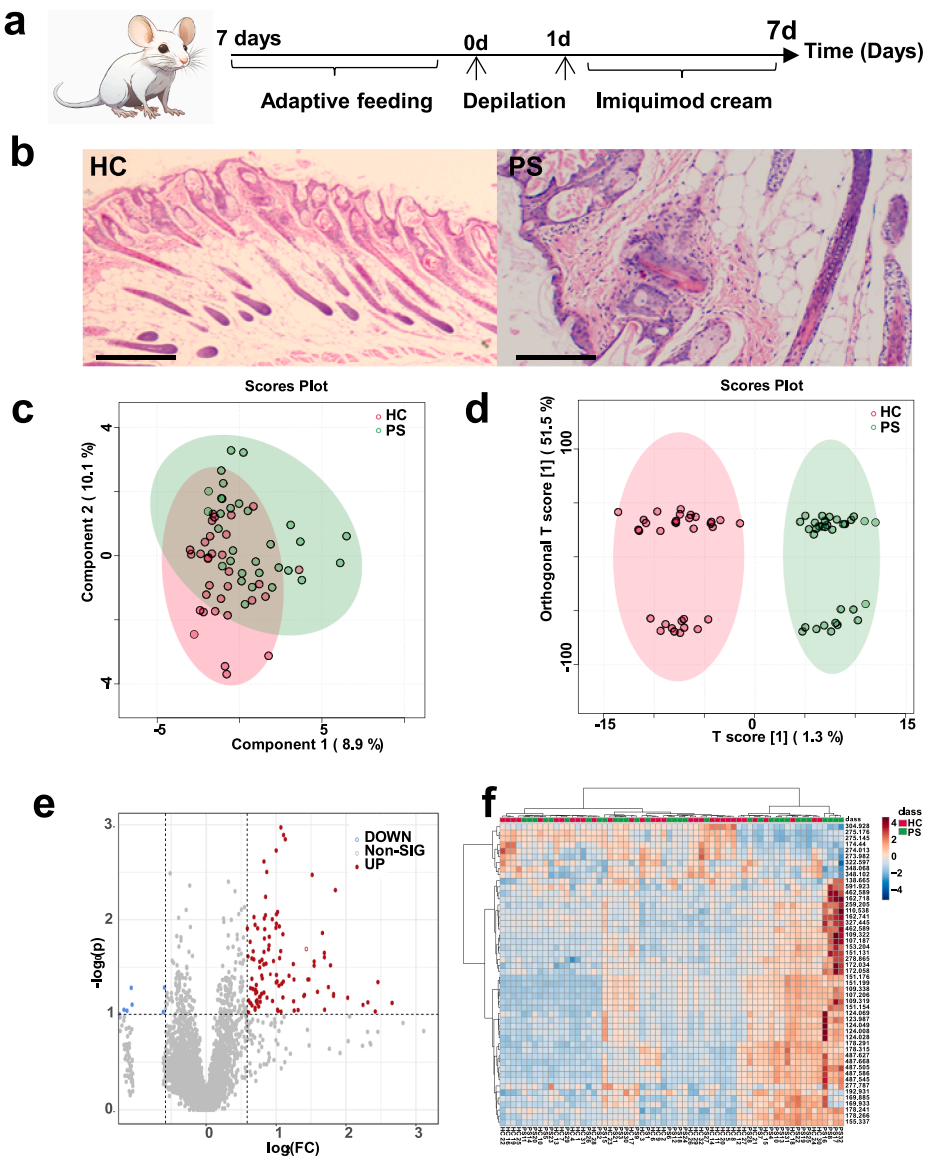


**Fig. 5.** MXene/MWCNTs LDI-MS-based metabolomic fingerprinting of serum biosamples of psoriasis animal model. a) Establishment of the psoriasis animal model through imiquimod application. b) Histopathological images of mouse skin before and after model establishment, highlighting the impact of imiquimod on epidermal texture and confirming successful model creation. c) PCA and d) OPLS-DA analyses distinguishing control and psoriasis groups among animal model samples. e) Volcano plot analysis of 32 control and 32 psoriasis animal model serum biosamples, with blue and red representing downregulated and upregulated molecules, respectively. f) Heatmap analysis of control and psoriasis groups, highlighting the differences between the two groups.

biosamples from the psoriasis animal model, harnessing Laser Desorption/Ionization Mass Spectrometry (LDI-MS) to unearth metabolic fingerprints. The establishment of the psoriasis animal model, carefully executed through imiquimod application, is graphically represented in Fig. 5a. The transformative impact of this approach on the epidermal landscape is vividly portrayed in histopathological images presented in Fig. 5b, corroborating the successful establishment of the psoriasis model. Intricacies of infiltrative erythema, silvery-white scales, and scattered bleeding spots encapsulate the visual cues of psoriasis-like manifestations on the murine canvas post-model creation. In a symphony of analytical techniques, Fig. 5c-d resonated with the successful differentiation of serum samples originating from 32 control mice and 32 mice representing the psoriasis model. The ensuing crescendo of potential biomarkers found visual embodiment through volcano plots (Fig. 5e) and heatmaps (Fig. 5f), echoing our resolute commitment to dissecting psoriasis-specific metabolic variances at the animal model stratum.

### 3.4. *Diagnostic performance and biomarker analysis of psoriasis*

Fig. 6a-B reflected our meticulous diagnostic performance evaluation viaReceiver Operating Characteristic (ROC) curve analysis, a strategy that scrutinizes the sensitivity and specificity of classification models across varied thresholds. Impressively, our metabolomic approach presented robust diagnostic efficacy in clinical and animal model samples, epitomized by Area Under the Curve (AUC) values of 0.959 and 0.924, respectively. This resounding endorsement attests to the potency of our methodology in bestowing diagnostic precision to psoriasis. Venturing further into the realm of metabolite analysis, we spotlight two key players-arachidonic acid and leukotriene E4. Fig. 6c and Fig. 6e showcased the elevation of these metabolites in psoriasis patients, their diagnostic potential further bolstered by impressive AUC analyses (Fig. 6d and Fig. 6f).

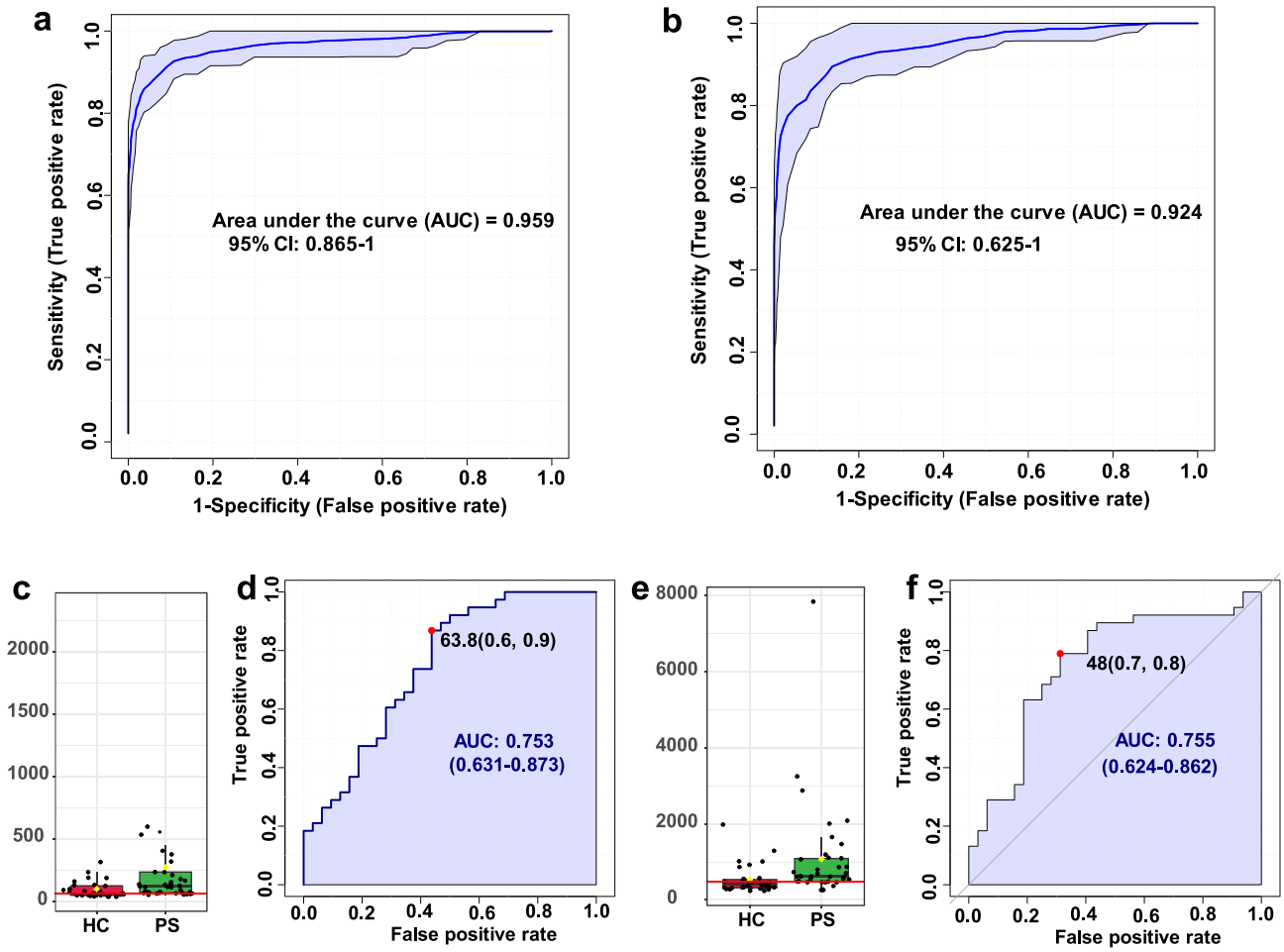


**Fig. 6.** Diagnostic performance and biomarker analysis of psoriasis using LDI-MS-based metabolomic approach with MXene/MWCNTs. a) Diagnostic performance of clinical samples, and b) diagnostic performance of animal model samples. Analysis of c) arachidonic acid intensity and d) area under the curve (AUC) in control and psoriasis groups. Analysis of e) leukotriene E4 intensity and f) AUC in control and psoriasis groups.

### *3.5. Validation of biomarkers and analysis of metabolic pathways*

In pursuit of more profound insights, we gaze upon the intriguing landscape of metabolic pathways, particularly the role of arachidonic acid and its intricate cascade. As revealed through PCR amplification, the expression of 5-LO and LTC4s in the psoriasis group underscores the dynamic role of the arachidonic acid pathway. This pathway serves as a conduit for transforming arachidonic acid into bioactive entities, orchestrating inflammation and immune modulation. In a harmonious choreography, LTC4s emerge as a pivotal player, converting arachidonic acid into leukotriene E4, a potent member of the leukotriene family implicated in processes ranging from inflammation to cellular signalling. Notably, the heightened expression of 5-LO and LTC4s within the psoriasis group amplifies the salience of the arachidonic acid pathway in psoriasis (Fig. 7a). In the panoramic vista of enrichment pathway analysis, as depicted in Fig. 7b, the arachidonic acid pathway emerges as a prominent presence, intricately interwoven with a constellation of metabolic pathways. This complex interplay elucidates the pivotal role of arachidonic acid and its associated pathways in the psoriasis narrative (Fig. 7c), affording profound insights into its occurrence, progression, and potential avenues for therapeutic intervention.

## 4. Conclusions

In this work, we proposed the strategy of incorporating multi-walled carbon nanotubes into transition metal carbides with unique morphology for screening the metabolic fingerprint of psoriasis. The distinctive hallmark of this strategy resides in the intricate design of MWCNTs-doped MXene, an approach that lends itself to the augmentation of the detection efficacy for perturbed metabolic moieties present in the intricate milieu of bodily fluids intricately linked with psoriasis. We have proficiently verified the two-dimensional configuration and elemental composition of MWCNTs-doped MXene, which tangibly validates the amplification of its LDI performance. We have achieved diagnostic efficiencies of 0.959 and 0.924 for discrete psoriasis from the control cohort via animal models and clinical biosamples. The discerning insights from enrichment pathway analysis have spotlighted the substantial upregulation of leukotriene E4 and arachidonic acid within the psoriasis cohort, accentuating their profound relevance. The consistency of mRNA expression validation of enzymes associated with these metabolic cascades affirmed a strong correlation, leading us to postulate that the perturbation of leukotriene metabolism might be implicated in the pathogenesis of psoriasis, thereby providing an opportunity to comprehend the occurrence and progression of psoriasis.

## 5. Informed consent statement

Informed consent was obtained from all subjects involved in the investigation. The Ethics Committee of Nanjing Medical University approved this investigation (2023-ab-201).

## CRediT authorship contribution statement

**Jun Chen:** Conceptualization. **Fang Liu:** Methodology. **Haibo Liu:**

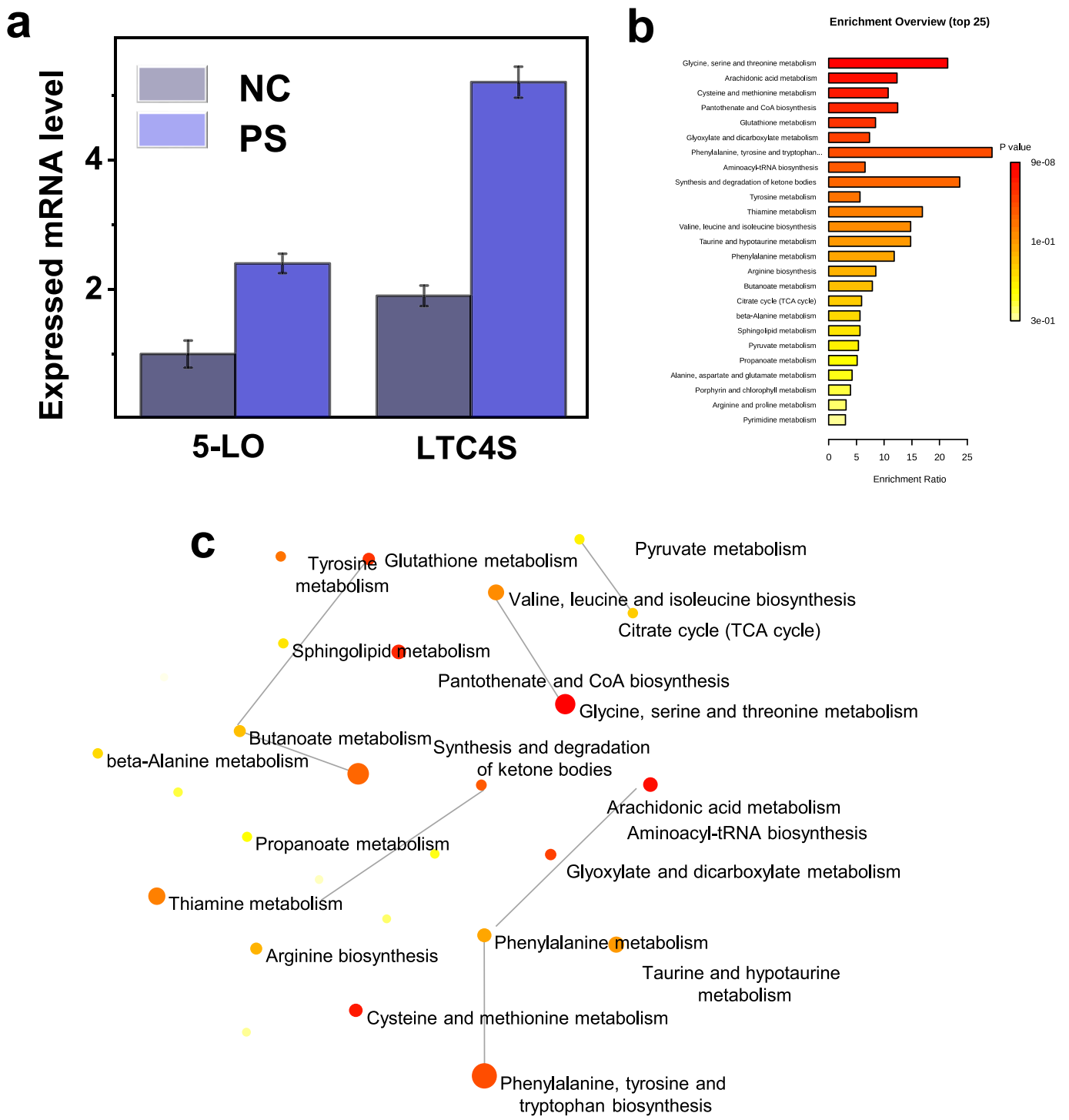


**Fig. 7.** Validation of biomarkers and exploration of related metabolic pathways. a) mRNA expression levels of 5-LO and LTC4s in control and psoriasis groups. b) Enrichment pathway analysis associated with psoriasis, and c) corresponding metabolic pathway network, with arachidonic acid significantly highlighted and exhibiting significant p-values.

Investigation. **Tengrui Wang:** Formal analysis. **Yun Hui:** Data curation. **Huan Chen:** Software. **Qingtao Kong:** Writing – review & editing.

## Declaration of competing interest

The authors declare that they have no known competing financial interests or personal relationships that could have appeared to influence the work reported in this paper.

## Appendix A. Supplementary material

Supplementary data to this article can be found online at https://doi.org/10.1016/j.arabjc.2024.105774.

## References

Abbasi, N.M., Xiao, Y., Peng, L., Duo, Y., Wang, L., Zhang, L., Wang, B., Zhang, H., 2021. Recent advancement for the synthesis of MXene derivatives and their sensing

protocol. Adv. Mater. Technol. 6, 202001197. https://doi.org/10.1002/admt.202001197.
Chen, J., Li, Y., Jiang, Y., Mao, L., Lai, M., Jiang, L., Liu, H., Nie, Z., 2021. TiO2/MXene-assisted LDI-MS for urine metabolic profiling in urinary disease. Adv. Funct. Mater. 31, 1–9. https://doi.org/10.1002/adfm.202106743.
Eom, W., Shin, H., Ambade, R.B., Lee, S.H., Lee, K.H., Kang, D.J., Han, T.H., 2020. Large-scale wet-spinning of highly electroconductive MXene fibers. Nat. Commun. 11, 2. https://doi.org/10.1038/s41467-020-16671-1.
Gao, K., Yang, R., Zhang, J., Wang, Z., Jia, C., Zhang, F., Li, S., Wang, J., Murtaza, G., Xie, H., Zhao, H., Wang, W., Chen, J., 2018. Effects of Qijian mixture on type 2 diabetes assessed by metabonomics, gut microbiota and network pharmacology. Pharmacol. Res. 130, 93–109. https://doi.org/10.1016/j.phrs.2018.01.011.
Hamdi, A., Hosu, I.S., Addad, A., Hartkoorn, R., Drobecq, H., Melnyk, O., Ezzaouia, H., Boukherroub, R., Coffinier, Y., 2017. MoS2/TiO2/SiNW surface as an effective substrate for LDI-MS detection of glucose and glutathione in real samples. Talanta 171, 101–107. https://doi.org/10.1016/j.talanta.2017.04.061.
Hosseini, E., Arjmand, M., Sundararaj, U., Karan, K., 2020. Filler-free conducting polymers as a new class of transparent electromagnetic interference shields. ACS Appl. Mater. Interfaces 12, 28596–28606. https://doi.org/10.1021/acsami.0c03544.
Hu, P., Wang, M., Gao, H., Zheng, A., Li, J., Mu, D., Tong, J., 2021. The role of helper T cells in psoriasis. Front. Immunol. 12, 34975883. https://doi.org/10.3389/fimmu.2021.788940.
Jiang, Z., Chen, Q., Zheng, Q., Shen, R., Zhang, P., Li, X., 2021. Constructing 1d/2d schottky-based heterojunctions between mn0.2cd0.8s nanorods and ti3c2 nanosheets for boosted photocatalytic h2 evolution. Wuli Huaxue Xuebao/ Acta Phys. - Chim. Sin. 37, 12. https://doi.org/10.3866/PKU.WHXB202010059.
Kailasa, S.K., Wu, H.F., 2015. Nanomaterial-based miniaturized extraction and preconcentration techniques coupled to matrix-assisted laser desorption/ionization mass spectrometry for assaying biomolecules. TrAC - Trends Anal. Chem. 65, 54–72. https://doi.org/10.1016/j.trac.2014.09.011.
Lai, J., Wang, T., Wang, H., Shi, F., Gu, W., Ye, L., 2018. MnO nanoparticles with unique excitation-dependent fluorescence for multicolor cellular imaging and MR imaging of brain glioma. Microchim. Acta 185, 29610993. https://doi.org/10.1007/s00604-018-2779-5.
Li, F., Liu, Y., Shi, X., Li, H., Wang, C., Zhang, Q., Ma, R., Liang, J., 2020. Printable and stretchable temperature-strain dual-sensing nanocomposite with high sensitivity and perfect stimulus discriminability. Nano Lett. 20, 6176–6184. https://doi.org/10.1021/acs.nanolett.0c02519.
Malik, R., Parida, R.K., Parida, B.N., Nayak, N.C., 2022. EMI shielding behavior of 2D-layered Ti3C2Tx (MXene) incorporated EMA/EOC ternary blend nanocomposites in S-band. J. Mater. Sci. Mater. Electron. 33, 22599–22613. https://doi.org/10.1007/s10854-022-09038-3.
Mugo, S.M., Alberkant, J., 2020. Flexible molecularly imprinted electrochemical sensor for cortisol monitoring in sweat. Anal. Bioanal. Chem. 412, 1825–1833. https://doi.org/10.1007/s00216-020-02430-0.
Naguib, M., Mashtalir, O., Carle, J., Presser, V., Lu, J., Hultman, L., Gogotsi, Y., Barsoum, M.W., 2012. Two-dimensional transition metal carbides. ACS Nano 6, 1322–1331. https://doi.org/10.1021/nn204153h.
Pinget, G.V., Tan, J.K., Ni, D., Taitz, J., Daien, C.I., Mielle, J., Moore, R.J., Stanley, D., Simpson, S., King, N.J.C., Macia, L., 2022. Dysbiosis in imiquimod-induced psoriasis alters gut immunity and exacerbates colitis development. Cell Rep. 40, 35977500. https://doi.org/10.1016/j.celrep.2022.111191.
Raharja, A., Mahil, S.K., Barker, J.N., 2021. Psoriasis: A brief overview. Clin. Med. J. R. Coll. Physicians London 21, 170–173. https://doi.org/10.7861/CLINMED.2021-0257.
Shang, M., Chen, X., Li, B., Niu, J., 2020. A fast Charge/discharge and wide-temperature battery with a germanium oxide layer on a Ti3C2 MXene matrix as anode. ACS Nano 14, 3678–3686. https://doi.org/10.1021/acsnano.0c00556.
Sotiriou, E., Tsentemeidou, A., Bakirtzi, K., Lallas, A., Ioannides, D., Vakirlis, E., 2021. Psoriasis exacerbation after COVID-19 vaccination: a report of 14 cases from a single centre. J. Eur. Acad. Dermatol. Venereol. 35, e857–e859. https://doi.org/10.1111/jdv.17582.
Wang, W., Kou, J., Zhang, M., Wang, T., Li, W., Wang, Y., Xie, Q., Wei, M., 2023. A metabonomic study to explore potential markers of asymptomatic hyperuricemia and acute gouty arthritis. J. Orthop. Surg. Res. 18, 36782295. https://doi.org/10.1186/s13018-023-03585-z.
Wang, P., Shah, G.L., Landau, H., Coulter, M.E., Walsh, C.A., Roider, E., Kramer, C.S., Beuning, P.J., Giese, R.W., 2020. Jettison-MS of nucleic acid species. J. Am. Soc. Mass Spectrom. 31, 1641–1646. https://doi.org/10.1021/jasms.0c00084.
Wang, S., Xu, J., Wang, W., Wang, G.J.N., Rastak, R., Molina-Lopez, F., Chung, J.W., Niu, S., Feig, V.R., Lopez, J., Lei, T., Kwon, S.K., Kim, Y., Foudeh, A.M., Ehrlich, A., Gasperini, A., Yun, Y., Murmann, B., Tok, J.B.H., Bao, Z., 2018. Skin electronics from scalable fabrication of an intrinsically stretchable transistor array. Nature 555, 83–88. https://doi.org/10.1038/nature25494.
Wu, W., Zhao, N., 2019. Metabolomics of Lactic Acid Bacteria. Lact. Acid Bact. Omi. Funct. Eval. 167–182. doi: 10.1007/978-981-13-7832-4_6.
Yang, H., Xiao, X., Li, Z., Li, K., Cheng, N., Li, S., Low, J.H., Jing, L., Fu, X., Achavananthadith, S., Low, F., Wang, Q., Yeh, P.L., Ren, H., Ho, J.S., Yeow, C.H., Chen, P.Y., 2020. Wireless Ti3C2TxMXene strain sensor with ultrahigh sensitivity and designated working windows for soft exoskeletons. ACS Nano 14, 11860–11875. https://doi.org/10.1021/acsnano.0c04730.
Zeng, Z., Wang, C., Siqueira, G., Han, D., Huch, A., Abdolhosseinzadeh, S., Heier, J., Nüesch, F., Zhang, C., Nyström, G., 2020. Nanocellulose-MXene biomimetic aerogels with orientation-tunable electromagnetic interference shielding performance. Adv. Sci. 7 https://doi.org/10.1002/advs.202000979.
Zhang, B., Lai, R.C., Sim, W.K., Choo, A.B.H., Lane, E.B., Lim, S.K., 2021. Topical application of mesenchymal stem cell exosomes alleviates the imiquimod induced psoriasis-like inflammation. Int. J. Mol. Sci. 22, 1–13. https://doi.org/10.3390/ijms22020720.
Zhang, J., Seyedin, S., Qin, S., Wang, Z., Moradi, S., Yang, F., Lynch, P.A., Yang, W., Liu, J., Wang, X., Razal, J.M., 2019. Highly conductive Ti 3 C 2 T x MXene hybrid fibers for flexible and elastic fiber-shaped supercapacitors. Small 15, e1804732. https://doi.org/10.1002/smll.201804732.
Zhang, Y.Z., Wang, Y., Jiang, Q., El-Demellawi, J.K., Kim, H., Alshareef, H.N., 2020. MXene printing and patterned coating for device applications. Adv. Mater. 32, 1–26. https://doi.org/10.1002/adma.201908486.
Zhang, Y., Zhang, L., Fan, X., Yang, W., Yu, B., Kou, J., Li, F., 2019. Captopril attenuates TAC-induced heart failure via inhibiting Wnt3a/β-catenin and Jak2/Stat3 pathways. Biomed. Pharmacother. 113, 108780 https://doi.org/10.1016/j.biopha.2019.108780.
Zhou, X., Chen, Y., Cui, L., Shi, Y., Guo, C., 2022. Advances in the pathogenesis of psoriasis: From keratinocyte perspective. Cell Death Dis. 13, 35075118. https://doi.org/10.1038/s41419-022-04523-3.
Zhu, W., Panda, S., Lu, C., Ma, Z., Khan, D., Dong, J., Sun, F., Xu, H., Zhang, Q., Zou, J., 2020. Using a self-assembled two-dimensional MXene-based catalyst (2D-Ni@Ti3C2) to enhance hydrogen storage properties of MgH2. ACS Appl. Mater. Interfaces 12, 50333–50343. https://doi.org/10.1021/acsami.0c12767.